Experimental Validation of the Predicted Performance of a Wind Driven Venturi Ventilator

M. A. Serag-Eldin

Abstract—The paper presents the results of simple measurements conducted on a model of a wind-driven venturi-type room ventilator. The ventilator design is new and was developed employing mathematical modeling. However, the computational model was not validated experimentally for the particular application considered. The paper presents the performance of the ventilator model under laboratory conditions, for five different wind tunnel speeds. The results are used to both demonstrate the effectiveness of the new design and to validate the computational model employed to develop it.

Keywords—Venturi-flow, ventilation, Wind-energy, Wind flow.

I. INTRODUCTION

IN a previous study, a new design for a wind driven venturi-type ventilator was presented [1]. The design was developed entirely employing computational modeling. However, the design was never tested experimentally. In the current work a physical model is built and its performance is tested experimentally. Moreover the computational model employed to develop the design is presented and validated with the aid of the measured data. The computational model is also employed to predict and reveal key features of the flow field encountered during the experiment.

The two main objectives of the current investigation are thus:

 i) demonstrate experimentally the operation of the new ventilator design.

 ii) validate a computational model which may be employed to further develop the design and to predict its performance under simulated real life conditions [2].

As the name implies, the ventilator design investigated here exploits the venturi principle. Fig. 1 displays a sketch of an isometric cut through the mid-plane of the device.

Atmospheric wind is guided into a converging channel to increase its speed and decrease its pressure. The minimum pressure occurs near the throat section; this partial vacuum is then employed to draw in air from the enclosure to be ventilated.

M. A. Serag-Eldin is with the Mechanical Engineering Department, American University in Cairo, Cairo, Egypt (phone: 202-27975324; fax: 202-27957565; e-mail: amrserag@aucegypt.edu).
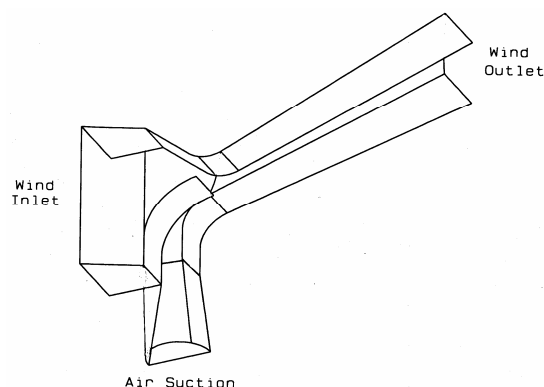
Fig. 1 Isometric sketch of mid-plane cut of wind-ventilator

In the following sections of the paper the experimental rig and measurement procedure are described, and the experimental results are displayed. The computational model is presented, and applied to predict the flow field occurring under experimental conditions; key features of the flow field are displayed. Corresponding measured and computed results are then compared and discussed. Finally a discussion and conclusion is made.

II. THE EXPERIMENT

A. The Experimental Rig

A sketch of the experimental rig, with the tunnel and model contours drawn to scale, is shown in Fig. 2; dimensions are in cms. The rig features an induced draft wind tunnel with an extended inlet section. The wind tunnel inlet displays a smooth bell-mouth followed by a uniform square section of 0.77 m sides and 0.90 m length. The ventilator model is fixed to the floor of the inlet section with its suction pipe extending downwards and protruding out of the wind tunnel bottom. The model suction pipe is approximately 51 m.m. in diameter. It features a bell mouthed inlet followed by a 45 cms straight length of pipe, followed by a venturi-meter with a 32 m.m. throat diameter. The venturi-meter is connected directly to the ventilator inlet section. It is employed to measure the inlet suction flow rate, with the aid of an inclined manometer. At its widest point (inlet to the guide vanes) the model width is 11 cm and its maximum height above the floor of the inlet

World Academy of Science, Engineering and Technology
International Journal of Aerospace and Mechanical Engineering
Vol:2, No:4, 2008

section is 41 cm. The frontal area of the model including the suction pipe is approximately 4 % of the inlet section area.
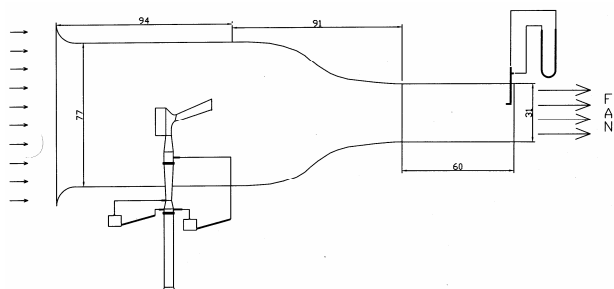

Fig. 2 Sketch of experimental apparatus

A pitot-static tube connected to a vertical U-tube water manometer is employed to measure the flow velocity at the end of the long straight section of the tunnel following the convergent nozzle; this is the exit section displayed in Fig. 2. Originally the straight section was the designed working section of the tunnel; however it was decided to place the model at inlet section after modifying and extending it so as to host a larger model size. The straight section is square with 30.5 cm sides, and is 61 cms long. Beyond the exit section is the wind tunnel fan section (not displayed in Fig. 2).

Fig. 3 presents a photographic picture of the inlet section of the wind-tunnel with the model attached. Fig. 4 displays the profile of the wind-tunnel, and reveals the protruding suction pipe (painted black).
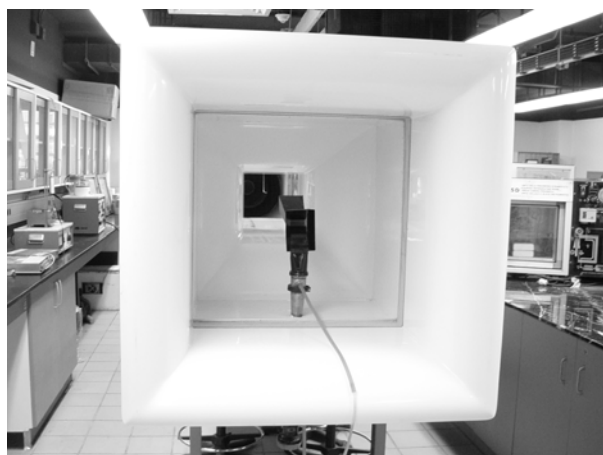

Fig. 3 Picture of the wind-tunnel inlet and model

B. Measurement Procedure

Prior to conducting the final runs some preliminary measurements were performed. First pitot-static tube traverses were conducted at the inlet plane of the model to measure uniformity of velocity profile at that section. This revealed the need to extend the inlet section of the wind tunnel in the initial set-up, and so the inlet section was extended sufficiently.

Similar traverses were conducted at the exit of the wind tunnel test section to check the uniformity of the flow at this section. This is necessary since this section serves as the exit

uniform-velocity-boundary in flow simulations. It is true that the wind tunnel is a commercial one and therefore designed to yield a uniform velocity profile at the test section, however, the presence of the upstream model causes partial obstruction to the flow. The checks, however, showed negligible velocity variations.
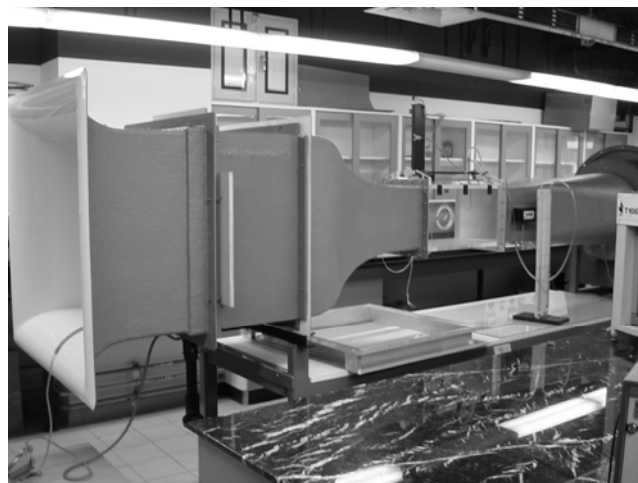

Fig. 4 Wind-tunnel profile and protruding suction pipe

Each run begins by starting the wind tunnel fan and fixing its speed electronically to a prescribed value. After steady state conditions are achieved, the pressure difference across the U-tube manometer connected to the pitot-static tube at the exit section is recorded. Simultaneously, the pressure-difference between the inlet and throat section of the venturi-meter on the suction pipe is recorded. In addition the pressure difference across the inlet and outlet of the venturi-meter is also recorded in order to measure the total pressure loss across the venturi section, required for CFD simulation of the flow.

For each measurement set, measurements are recorded for five different fan speeds; the fan speed increasing in step increments of 5 Hz starting with 40 Hz. Four different sets of measurements were made.

C. Measured Performance

The performance characteristics of the ventilator comprise the profile of the mean suction velocity V_{suc}, versus the upstream velocity W_{in}. The former is derived from the suction flow rate divided by inlet area; whereas the latter is calculated from the measured exit section velocity employing the continuity equation.

Fig. 5 displays the results of the four sets of measurements, together with a trend line for each. The results are seen to be in close agreement; minor deviations are present which are possibly due to limited accuracy and resolution of measuring equipment, fluctuations in fan speed, and differences in air temperature during measurements. However they all display very close trend lines, despite the fact that the measurements were conducted on different days, the last a couple of weeks after the first. Higher accuracy was not deemed necessary for the current purpose.
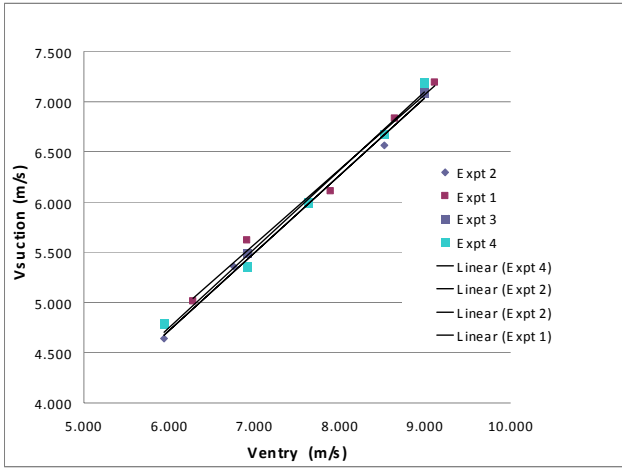
World Academy of Science, Engineering and Technology
International Journal of Aerospace and Mechanical Engineering
Vol:2, No:4, 2008

Fig. 5 Measured Performance of ventilator model

It is noticed that the profiles indicate a near linear relation between V_{suc} and W_{in}. This is explained as follows: the pressure drop in the venturi-throat section is proportional to W_{in}^2, and the pressure drop in the suction pipe and ducts to the throat section is proportional to V_{suc}^2; since, the former must approximately equal the latter, it should be expected that the V_{in} versus W_{in} relation is approximately linear.

III. THE MATHEMATICAL MODEL

A. Governing Equations and Grid System

The computational model comprises fully three-dimensional elliptic differential equations expressing conservation of mass, balance of momentum in three directions and transport of the kinetic energy of turbulence, k, and it's rate of dissipation, ε; the later two equations being introduced by the adopted Renormaliation Group(RNG) k-ε turbulence model [3],[4]. The equations are discretized employing a finite volume method ,e.g.[5] and solved by a variant of the SIMPLE algorithm [6].

In order to express the wall boundary conditions accurately, a three-dimensional, non-orthogonal boundary fitted coordinate system is employed [7]. Elliptic grid generation [8] is adopted to generate the Cartesian coordinates of the control volume corner points. Fig. 6 displays a part of the BFC grid in the vertical plane passing through the mid-section of the ventilator. Since the view is two- dimensional, it displays only two sets of grid-lines, namely the J and K grid lines. It is noticed that some of the grid lines have been shaped to fit the ventilator contours exactly.

Since the coordinate system is curvilinear, the grid-line orientations vary continuously, the J and K grid-lines coinciding with the vertical and stream-wise directions, respectively, at the inlet and exit boundaries only. The third grid-line set I, represents the lateral cross-stream direction and is normal to the other two at the inlet, exit, symmetry and side boundary planes only. It is noticed that the grid-lines are too densely packed in some regions to be discernable. The compacting of grid lines is due to the need for high resolution in certain regions, as well as the outcome of the grid curvature

required to give a high level of grid orthogonality. Due to symmetry the integration domain covers only one half of the wind-tunnel cross-section.
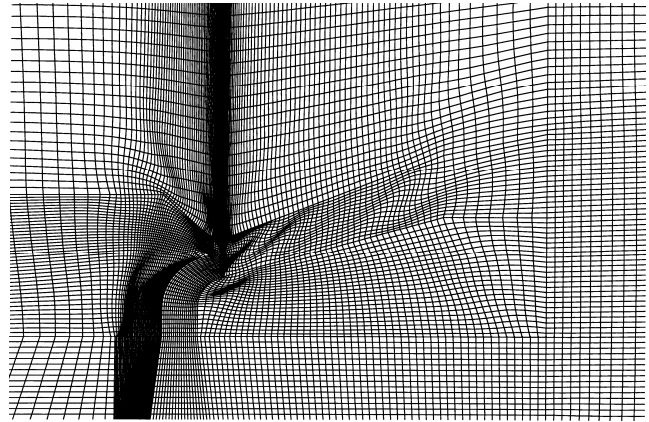

Fig. 6 Boundary-fitted-coordinates surrounding ventilator

Details of expressing the convection and diffusion terms in boundary fitted coordinates may be found in [9],[10]; essentially, the control volume equations state:

$$C_\phi = D_\phi + S_\phi \qquad (1)$$

where C_ϕ expresses the net rate of convection of the variable φ out of the control volume, D_ϕ expresses the net rate of diffusion of φ into the control volume, and S_ϕ expresses the sum of sources of φ within the control volume. The mass conservation equation may also be expressed in the form of (1) with no diffusion nor source terms. For the momentum equations the source terms represent the pressure gradient terms, whereas for the k -equation the source terms represent the difference between the generation and dissipation rates. For the ε-equation the source term is $S_\varepsilon = [C_1 G_{k-} C_2 \rho\varepsilon] \varepsilon/k.$ + R, where G_k denotes the generation rate of k, C_1 and C_2 are turbulence model constants whose values are displayed with the other model constants in Table I, and R denotes the source term from renormalization. The latter is expressed by the following relation:

$$R = \rho \frac{C_\mu \eta^3 (1-\eta/\eta_o)}{1+\beta\eta^3} \frac{\varepsilon^2}{k} \qquad (2)$$

where:

$$\eta = S\frac{k}{\varepsilon}, \quad S = (2S_{ij}S_{ij})^{1/2}, \quad S_{ij} = \frac{1}{2}(\frac{\partial u_i}{\partial x_j}+\frac{\partial u_j}{\partial x_i}) \quad (3)$$

The momentum diffusion terms employ a velocity gradient expression with an eddy diffusivity, μ_t derived from k and ε according to:

$$\mu_t \equiv \rho\ C_\mu\ k^2 /\varepsilon \qquad (4)$$

where C_μ is another turbulence model constant. The eddy diffusivity terms for k and ε are expressed by μ_t/σ_k and μ_t/σ_ε, respectively , σ_k and σ_ε being turbulence model constants.

World Academy of Science, Engineering and Technology
International Journal of Aerospace and Mechanical Engineering
Vol:2, No:4, 2008

TABLE I
TURBULENCE MODEL CONSTANTS

C_1	C_2	C_μ	σ_k	σ_ε	β	η_o
1.42	1.68	.0845	0.7194	0.7194	0.012	4.38

B. Boundary Conditions

The integration domain follows the contours of the wind-tunnel from inlet to the end of the test section, terminating immediately upstream the fan duct. The boundary conditions are specified to represent the experimental conditions as faithfully as possible. The following type of boundaries and conditions are encountered:

1) Inlet boundary

This corresponds to the wind tunnel inlet section, right after the bell mouth. A total pressure boundary condition is imposed there; with the total pressure equal to atmospheric pressure and the inlet axial velocity component solved for. The fluid is assumed to enter with negligible cross-stream and vertical velocity components, and with a uniform value of k equal to 1% of the inlet mean flow kinetic energy. The inlet value of ε is calculated from the inlet value of turbulence and a length scale equal to 0.4* average distance from wall boundaries(quarter height of inlet section).

2) Wall boundaries

These comprise the inner walls of the wind tunnel, and both the inner and outer walls of the model. No slip, smooth wall, equilibrium wall functions are applied at those boundaries [11]. They imply the calculation of the wall shear stress from a logarithmic function.

3) Exit section

This corresponds to the downstream-end of the original wind-tunnel test-section, the section immediately upstream the fan section. A uniform value of W_{ex} is specified at this boundary, while the pressure is solved for. The value of W_{ex} is specified to be the experimentally measured one. The flow is assumed to leave this boundary with the same properties as for the immediate upstream plane.

4) Suction-pipe boundary

This corresponds to the suction pipe cross-section at the floor of the wind tunnel, and it is specified the same diameter as that of the ventilator inlet. The actual suction pipe used in the experiment extends further down than that, protruding a considerable distance below the wind tunnel floor, Fig. 2. Moreover it includes a bell mouthed inlet, straight length of piping, a venturi-meter, and an upstream and downstream sleeve to attach the venturi- meter to the pipe and model inlet, respectively.

However for the purpose of the present analysis the extra complication involved in protruding the integration domain and modeling the flow within the venturi-meter is considered unnecessary. Instead the flow losses between the inlet of the suction pipe and the inlet of the model are estimated from common practice as follows:

i) loss in the 45 cms length of pipe $= 0.192\ V_{suc}^2/2g$
ii) loss in the 2 sleeves $= 0.077\ V_{suc}^2/2g$
iii) loss in the venturi-meter $= 0.728\ V_{suc}^2/2g$

The total loss in the venturi-meter is actually based on experimental measurements at the highest wind speed. It equals approximately 11% of the measured pressure difference between venturi-throat and inlet. This compares well with the 10-15 % figure reported in the literature [12].

Therefore the total suction pipe loss is specified to be equal to $V_{suc}^2/2g$. A total pressure boundary condition is specified at this boundary with the total pressure equal to atmospheric pressure. The pressure drop due to the miscellaneous losses in the suction pipe is spread uniformly over the entire length of the pipe. The inlet suction velocity V_{suc} is solved for at the boundary, and the other velocity components are neglected. The inlet value of k is specified to be 1% of V_{suc}^2, and ε is calculated from that value of k and a length scale equal to 0.4 x average radius of pipe.

5) Symmetry plane

This is the vertical mid-plane of the ventilator. Symmetry boundary conditions are imposed at this boundary.

C. Predictions

1) *Grid-dependence*

Prior to comparing measurements and predictions it is prudent to conduct grid-independence checks. Table II reveals the results of key runs that were conducted for that purpose. The first column indicates the run number; the second , third, and fourth columns display the number of grid nodes employed in the I, J, and K-directions, NI, NJ and NK, respectively. The fifth column gives the total number of grid nodes NIJK; whereas the sixth column gives V_{suc}. The last column gives the nominal gradient; it represents, for a particular range of grid nodes, the derivative dV_{suc}/dN where N is the number of nodes in the I, J or K direction. Small values of this gradient indicate that further grid refinement will not change the result substantially, i.e. grid-independence of the solution.

TABLE II
GRID INDEPENDENCE RUNS

#	NI	NJ	NK	NIJK	V_{suc}	Gradient
1	27	86	113	262386	5.798	0.001530
2	34	109	142	526252	5.627	
#	NI	NJ	NK	NIJK	V_{suc}	Gradient
2	34	109	142	526252	5.627	0.000244
3	42	109	142	650076	5.629	
#	NI	NJ	NK	NIJK	V_{suc}	Gradient
2	34	109	142	526252	5.627	-0.001916
4	34	109	185	685610	5.545	-0.000366
5	34	109	211	781966	5.535	
#	NI	NJ	NK	NIJK	V_{suc}	Gradient
4	34	109	185	685610	5.545	0.000565
6	34	130	185	817700	5.557	

Successive rows in Table II generally display results of runs having equal number of grid nodes in two directions, and a different number in the direction considered (gradient direction). The first two rows however are an exception, since they display results of two runs with varying number of grid nodes in the three directions, albeit keeping the expansion ratios the same in all three directions. For comparison purposes the gradient in this case is defined as the change in V_{suc} divided by three times the change in the cube-root of

World Academy of Science, Engineering and Technology
International Journal of Aerospace and Mechanical Engineering
Vol:2, No:4, 2008

NIJK; this would yield the rate of change in any one direction if the rates of change in the three directions were identical.

Comparison of the V_{suc} results of runs #1 and #2 reveals considerable grid dependence of the results of run #1; hence the coarser grid will not be considered further. Comparison of results of run #3 and #2 reveals negligible change with increase of number of grid nodes in the I-direction NI; hence NI = 34 will be adopted for future runs.

Comparison of results of runs #2 and #4 reveals considerable grid dependence in the K-direction; indeed the K-direction gradient is an order of magnitude greater than the I-direction gradient. Increasing the number of grid nodes in the K-direction NK, to NK= 211 shows a marked improvement in grid-independence, and there is no reason to further refine the grid; hence NK=211 will be used for comparison runs.

Comparison of results of runs #4 and #6 reveals negligible grid independence and hence the number of grid nodes in the y-direction NJ, adopted for comparison will be NJ=109 nodes. Fig. 7 reveals the results of Table II in graphical form. The ordinate presents V_{suc} , whereas the abscissa denotes either NI, NJ,NK or NIJK, according to the profile displayed; the slopes of the lines indicate the gradients.
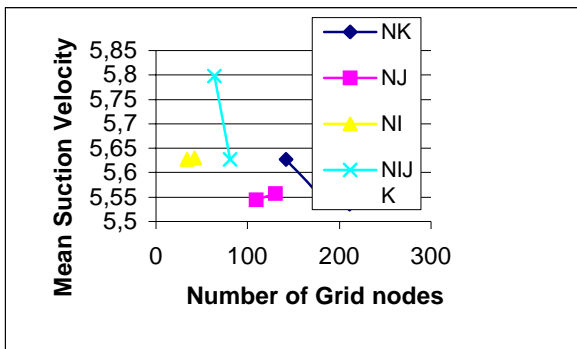

Fig. 7 Display of grid-dependence of results on grid size

The largest gradient accepted here is that in the y-direction and its magnitude is 0.000565 m/s/per NJ. Thus, if the gradient would remain constant with number of grid nodes, increasing NJ by 100 grid nodes would only result in a .0565 m/s increase in value of V_{suc}, which is approximately 1%. However, the expected increase would be much less since the magnitude of the gradient dies out quickly with increase of number of grid nodes, the NK curve in Fig. 7 being a typical example.

Moreover, since V_{suc} tends to increase with both NJ and NI, and decrease with NK, the grid-dependence errors tend to partially cancel out. Thus for all practical reasons the results may be assumed to be grid independent.

2) Convergence

Convergence was monitored by observing the change with iterations of both, the sum of absolute values of residuals, and the dependent variable values at a monitoring location; the latter being selected at the center of the suction pipe inlet. A total of 1500-2000 iterations were performed for each case, reducing sum of absolute mass-residuals by an order of 5-6 magnitudes, and stabilizing values of all dependent variables.

3) Sample Results

Fig. 8 reveals the predicted velocity vectors over a large section of the symmetry plane. Unfortunately because of the very fine grid employed in some regions the velocity vectors are too tightly packed to be discernible.
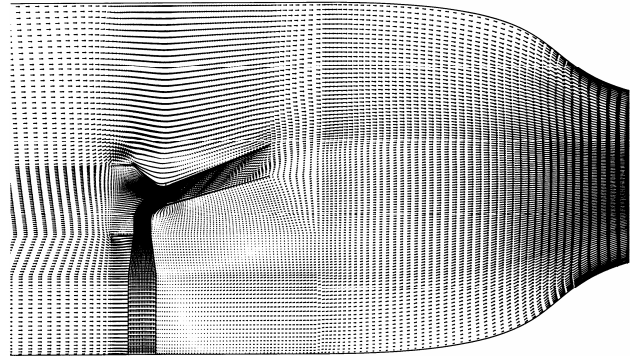

Fig. 8 Velocity vectors over a large section of mid-plane
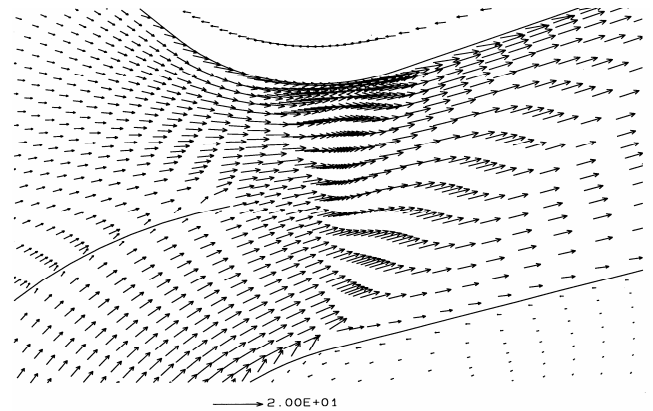

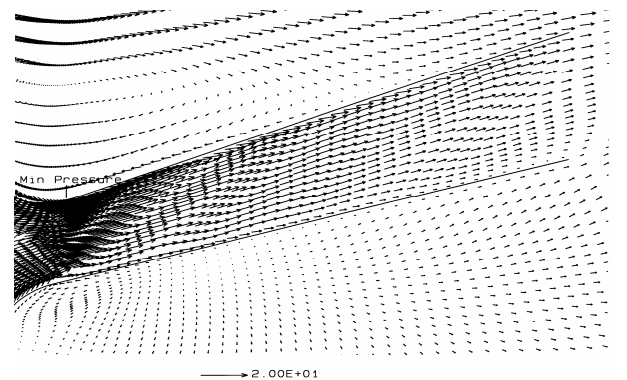Fig. 9 Velocity vectors in vicinity of throat

Fig. 10 Velocity vectors in diffuser section

Thus Fig. 9 displays a close-up of the velocity vectors in the immediate vicinity of the throat. The vectors reveal a smooth flow in this region with the wind stream and suction stream combining smoothly into one stream. The magnitudes of the vectors indicate a rapidly accelerating wind stream as the throat is reached. The magnitude of the suction stream

World Academy of Science, Engineering and Technology
International Journal of Aerospace and Mechanical Engineering
Vol:2, No:4, 2008

vectors shows that the suction velocities are comparable in magnitude to the wind stream velocity at this section.

Fig. 10 reveals the corresponding vectors in the diffuser section of the ventilator. It is seen that the combined wind and suction streams flows smoothly down the diffuser, reducing its speed and recovering some of the venturi pressure-drop. Flow separation is not observed. This smooth flow and pressure recovery feature is essential for lowering the pressure at the throat section and therefore increasing the suction air flow rate(the criteria for performance).

Fig. 11 displays the pressure contour lines at the throat section. The pressure increments are constant and therefore close spacing of the lines indicates large pressure gradients. Very high gradients appear on the top wall boundary in the throat section. The minimum pressure occurs at a point slightly downstream the section where the two streams meet, and is ideally located to draw in both the wind stream and suction air stream. The pressure contour lines upstream the throat is observed to be normal to the incoming wind stream, implying longitudinal acceleration. However, the pressure contour lines towards the end of the suction passage are noticeably inclined to the suction air stream, due to the effect of the centrifugal acceleration as the flow turns round the bend.
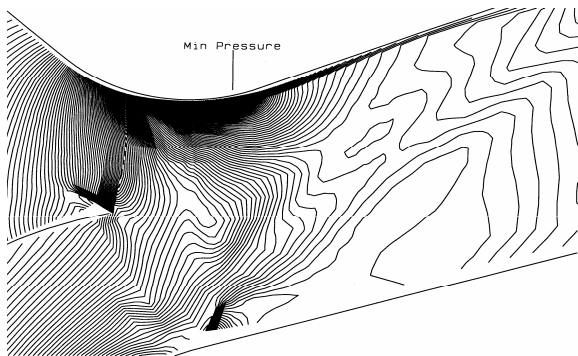

Fig. 11 Pressure contour lines at throat section

Fig. 12 reveals the corresponding contour lines within the diffuser section of the ventilator. For the most part, it shows almost parallel lines which are normal to the main flow direction indicating smooth flow and absence of separation. The exception being at the upstream end of the diffuser where the two streams join, and at the exit of the diffuser where the diffuser stream meets the external wind.
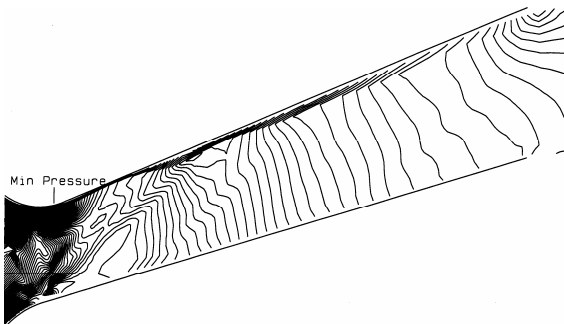

Fig. 12 Pressure contour lines in diffuser section

IV. COMPARISON OF MEASURED AND PREDICTED PERFORMANCE

The measured results are displayed together with the corresponding predicted ones in Fig. 13. Two prediction lines are displayed; one corresponding to the boundary conditions as stated earlier, and the other featuring a 15% reduction in the total pressure loss within the suction pipe. The latter line is indicated by the cf=0.85 annotation, and was introduced mainly to investigate the sensitivity of predictions to inlet losses. Both sets of predictions display exactly the same trend as the measurements. The cf=0.85 line reveals excellent agreement whereas the original set of predictions reveal only good agreement; consistently under estimating V_{suc}.

This could be attributed to either an over prediction of flow resistance by the turbulence model and adopted wall functions, measurement errors, grid-dependence effects , small differences in the boundary conditions, or a combination of all these factors. The differences in boundary conditions may be most pronounced at the inlet to the ventilator suction pipe, and the predicted values of V_{suc} are particularly sensitive to it, as revealed in Fig. 13.
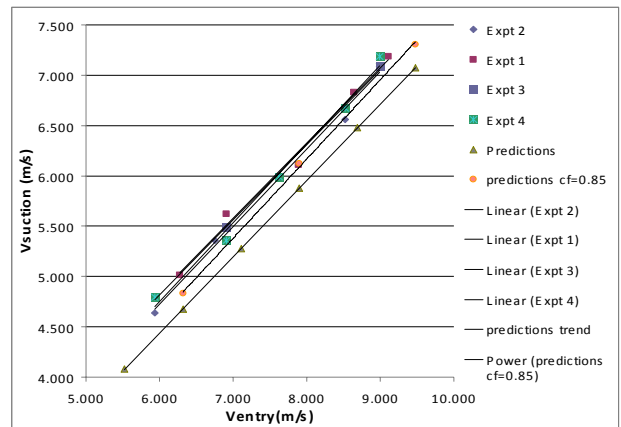

Fig. 13 Comparison of measured and predicted results

V. DISCUSSION AND CONCLUSION

A simple experiment was set-up in order to measure the performance of a new venturi-ventilator design under laboratory conditions. The performance, which is defined by the mean suction velocity versus inlet wind speed relation, is measured and compared against corresponding predictions made by the computational model. The agreement is found to be good, thus validating the computational model employed.

Although the ventilator model in the experiment was enclosed inside a wind tunnel, whereas the prototype would be subject to open atmospheric conditions, the difference between the two conditions is sufficiently small that the performance results obtained in the experiment would describe at least qualitatively the flow under actual operating conditions. To get quantitatively accurate performance curves under diversified conditions simulating more closely the actual operating conditions, it is recommended to employ the validated computational model.

REFERENCES

[1] M.A. Serag-Eldin, "Aerodynamic Design of a 3-D Ventilation Device for Stationary Enclosures," *PHOENICS Jr. of Computational Fluid Dynamics and its Applications,* vol.14, No.2, pp.159-177, 2001.

[2] M.A. Serag-Eldin, "Prediction of Performance of a Wind-Driven Ventilation Device," JWEIA, submitted for publication,2007.

[3] V. Yakhot and S. Orszag, "Renormalization Group Analysis of Turbulence. I.Basic Theory," *J. of Scientific Computing*, vol.I , No.1, pp.3-51.,1986.

[4] V. Yakhot and L.M. Smith, " The Renormalization Group, the ε-expansion and Derivation of Turbulence Models," J. of Scientific Computing, vol. 7, No.1., pp. , 1992.

[5] J.H. Ferziger and M. Peric, *Computational Methods for Fluid Dynamics*, 2nd edition. New York: Springer-Verlag, 1999.

[6] L.S. Carreto, A.D. Gosman, S.V. Patankar and D.B. Spalding, "Two Calculation Procedures for Steady Three-Dimensional Flow with Recirculation," Proceedings of the 3rd Int. Conf. Num. Methods in Fluid Mechs., vol II, pp.60-98, 1973,.

[7] J.F. Thompson, Z.U.Warsi and C.W. Mastin, "Boundary-fitted Coordinate Systems for Numerical Solution of Partial Differential Equations – A Review," *J. of Computational Physics*, vol.47, pp 1- 108, 1982.

[8] D.J. Anderson, *Computational Fluid Dynamics*, McGraw-Hill, London & New York, 1995.

[9] M.R. Malin, H.I.Rosten, D.B.Spalding and D.G.Tatchell, "Application of PHOENICS to Flow Around Ship's Hulls," Proceedings of 2nd Int. Symposium on Ship Viscous Resistance, Goteburg, Sweden, 1985.

[10] P.K. Hedberg, H.I.Rosten and D.B.Spalding, "The PHOENICS Equations", CHAM Report TR/99, CHAM U.K.

[11] B.E. Launder and D.B .Spalding, "The Numerical Computation of Turbulent Flows", *J. Computational Methods in Applied Mechanics and Eng.*, vol.3, pp. 269-289, 1974.

[12] E.O. Doebelin, Measurement Systems: Application and Design, McGraw-Hill: Tokyo, London and Sydney, p.472,Ch.7, 1976.